

Large amplitude behavior of the G rinfeld instability

Part II: The multi-cycloid model

Peter Kohlert and Klaus Kassner
Institut für Theoretische Physik,
Otto-von-Guericke-Universität Magdeburg,
Postfach 4120, D-39016 Magdeburg, Germany

Chaouqi Misbah
Groupe de recherche sur les Phénomènes hors de l'Équilibre,
LSP, Université Joseph Fourier (CNRS), Grenoble I,
B.P. 87, Saint-Martin d'Hères, 38402 Cedex, France
(Dated: May 21, 2019)

In a preceding paper [Phys. Rev. E, this volume, p. ...] we have carried amplitude expansions of the continuum equations for the G rinfeld instability to high orders. Nevertheless, the approach turned out to be restricted to relatively small amplitudes. In this article, we use a variational approach in terms of multi-cycloid curves instead. Besides its higher precision at given order, advantages of the method are that it gives a transparent physical meaning to the appearance of cusp singularities and is, in principle, not restricted to interfaces representable as single-valued functions. Using a single cycloid as ansatz function, the entire calculation can be performed analytically, which gives a good qualitative overview of the system. Taking into account several but few cycloid modes, we obtain remarkably good quantitative agreement with preceding numerically exact calculations. Our approach extends these calculations to situations involving gravity effects. Results on the shape of steady-state solutions are presented at both large stresses and amplitudes. In addition, their stability is investigated, including features that persist as the number of free parameters in the ansatz functions increases.

PACS numbers: 47.20.Hw, 05.70.Ln, 46.25.-y, 81.10.Aj
Keywords:

I. INTRODUCTION

Numerical simulations of a solid undergoing the G rinfeld instability [1, 2, 3] have the awkward tendency of producing cusp singularities in finite time. The investigation of Spencer and Meiron [3] has shown that these singularities are not an artifact of the numerics but intrinsic to the continuum model describing the system, under the assumption of linear elasticity in the limit of negligible sound propagation effects. What they found was a steady branch of solutions in a certain range of wavelengths, corresponding to very small sinusoidal shapes near the onset of the branch and approaching a cycloid-like cuspy shape near its termination. Such a result might have been anticipated on the basis of the analytic work by Chiu and Gao [4], who performed a detailed calculation of the stress state under a cycloid-shaped surface using the Goursat function scheme proposed by Muechelschili [5].

They state that for a certain range of wavenumbers a fully cusped cycloid constitutes an energetically more stable configuration than a flat surface. In section II, we will show that a variational calculation using cycloids as ansatz functions gives a rather good approximation of the large amplitude behavior as proposed in [3]. Moreover,

we are able to draw conclusions on the large amplitude behavior even for strong gravity or a large density difference between the solid and nonsolid phases (liquid or vacuum), as we show in section III. Evidence for these states has already been found in [6], henceforth denoted as I.

In section IV, we will present a generalization of this idea. By application of a special system of functions called multi-cycloids we analytically recover the numerical results to excellent accuracy already at third order.

II. THE MONO-CYCLOID APPROXIMATION

A. Cycloids

Cycloids belong to the more generic class of trochoids, curves defined as the trace of a point fixed on a circle rolling along some prescribed line. A cycloid is the curve traced out by a point on the circumference of a circle as the latter rolls along a straight line. When we put the point inside or outside the circle instead, we obtain a curtate or a prolate cycloid, respectively. The parametric representation of a cycloid can be given in a compact manner by a complex generating function

$$z(\theta) = \frac{z_0}{k} e^{ik\theta}; \quad (1)$$

Herein, i is the imaginary unit, k is a wavenumber and η is a dimensionless amplitude-like parameter. The cycloid is obtained by taking the real and imaginary part as the x and y coordinates, respectively.

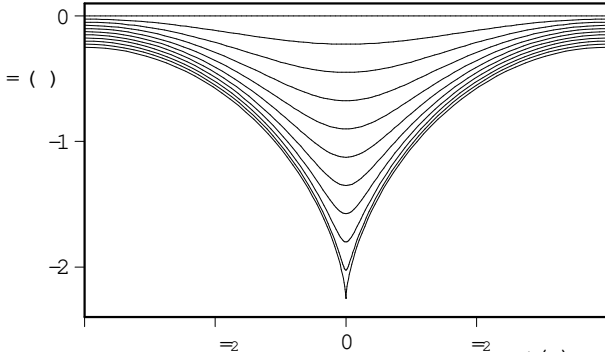


FIG. 1: Cycloids, as in equation (1) with $k = \frac{1}{2}$, plotted in the range $x \in (-1, 1)$; $\eta = 0 :: 1$ from top to bottom. The curves have been shifted in the y -direction in order to avoid overlapping.

Taking $\eta = 1$ leads to the representation of the classical, i.e., cusped, cycloid. Choice of a plus instead of the minus sign in equation (1) would just shift the minimum from $x = 0$ to $x = \pm k$, while a plus sign in the exponent would lead to a surface with the cusps pointing upward. The latter case is of no relevance for the Grinfeld instability, because a fully relaxed upward cusp would immediately shrink under any perturbation in order to decrease the surface energy.

For $\eta > 1$, the cycloid becomes self-intersecting and does not represent a physical state anymore. Note, however, that if we "superimpose" several cycloids [13] as we will do in section IV, the possibility of the x coordinate to increase nonmonotonously allows the representation of patterns with overhangs that do not self-intersect. We will not discuss this feature in detail here but report on those patterns in a different article.

The parametric representation of the cycloid is

$$x(\eta) = \frac{1}{k} \sin(k\eta); \quad (2a)$$

$$y(\eta) = \frac{1}{k} \cos(k\eta); \quad (2b)$$

In order to keep the average interface position at $y = 0$, we shift the cycloid position by its mean value, which is

$$m = \frac{k}{2} \int_0^{2\pi} \cos(k\eta) d\eta = \frac{2}{2k}; \quad (3)$$

where the dot denotes differentiation with respect to η , i.e., from now on we use

$$y(\eta) = \frac{1}{k} \cos(k\eta) - \frac{2}{2k}; \quad (4)$$

Moreover, if we want to compare results with both our previous calculation in I and the work of Spencer and

Meiron [3], we additionally have to know the mean square amplitude of the cycloid. In accordance with I, we call this mean square amplitude \bar{m} , and it is calculated by

$$\bar{m} = \frac{k}{2} \int_0^{2\pi} \cos^2(k\eta) d\eta = \frac{1}{2k}; \quad (5)$$

where the absolute value ensures a nonnegative mean square amplitude, no matter what the sign of k and of η .

B. Scaling

We have shown in I that the equations of motion of the Grinfeld instability can be made parameter free, if gravity is neglected. This is achieved by referring all lengths to a length scale l_1 , the Grinfeld length, given by:

$$l_1 = \frac{1}{2w_0}; \quad (6)$$

where $w_0 = \frac{1}{2} (1 - \eta^2) = 2E$, which is the elastic energy density of the prestressed planar state [7]. When gravity is considered, another length l_2 becomes important, which is

$$l_2 = \frac{w_0}{g}; \quad (7)$$

The only parameter of the nondimensionalized equations is the ratio of these length scales:

$$l_{12} = \frac{l_1}{l_2}; \quad (8)$$

So, in all considerations to follow, we have carried out a formal transformation $x \rightarrow x/l_1$, $y \rightarrow y/l_1$, $k \rightarrow kl_1$, $\eta \rightarrow \eta/l_1$, and energies and their variations have been divided by a common prefactor.

C. The cycloid approximation for the no-gravity case

We will not explicitly repeat the derivation of the energy terms given in I, because in treating the cycloid approximation, we choose a slightly different approach, which is essentially variational in nature. Therefore, we need not compute the energy itself but only its variation. (Of course, we could have done so in I as well, but since the energy computation is easier for a superposition of Fourier modes than for one of cycloids, we could avoid to compute the energy itself there.) The variation of strain energy due to a configurational variation x can be written as

$$E_e = \int w(s) dx; \quad (9)$$

where $w(s)$ is the energy density at the surface, \mathbf{n} is the normal vector and s denotes the arclength along the surface. Using Eqs. (2a) and (4) we can calculate an approximation to E_e , allowing only the parameter to vary (instead of taking the full variational derivative which would take the result out of the space of cycloidal shapes)

$$\begin{aligned} \mathbf{x} &= \frac{\partial x(\theta)}{\partial \theta} \mathbf{e}_x + \frac{\partial y(\theta)}{\partial \theta} \mathbf{e}_y \\ &= k^{-1} [\sin(k\theta) \mathbf{e}_x + (\cos(k\theta) + 1) \mathbf{e}_y] \end{aligned} \quad (10)$$

and we have the relation

$$\begin{aligned} \mathbf{n} ds &= (\underline{y}(\theta) \mathbf{e}_x + \underline{x}(\theta) \mathbf{e}_y) d\theta \\ &= [(1 - \sin(k\theta)) \mathbf{e}_x + (1 + \cos(k\theta)) \mathbf{e}_y] d\theta \end{aligned} \quad (11)$$

The calculation of the strain energy density will be given in appendix A for the general case of a multi-cycloid. Parts of this calculation have already been presented in [7], but at this point we only need the energy density for the mono-cycloidal surface:

$$w(s) = \frac{1}{2} \frac{1 + \frac{1}{2} \cos^2(k\theta)}{(1 + \frac{1}{2} \cos(k\theta))^2} \quad (12)$$

When comparing with the results of [4] one finds the only difference (up to prefactors) in the different sign of the cosine function, which results from their different ansatz of the generating function, corresponding to a simple shift of the argument of the cosine. The integration yields a surprisingly simple result:

$$\frac{\partial E_e}{\partial k} = \frac{1}{k} \int_0^1 w(s) \cos(k\theta)^2 d\theta = \frac{2}{k^2}; \quad (13)$$

where we have taken $k > 0$ (otherwise the expression on the right would have to be multiplied by the sign of k).

It remains to be noticed that the integration can be done analytically in the mono-cycloid case, giving

$$E_e = \frac{2}{k^2} \quad (14)$$

The surface energy in our scalings simply is the difference of the arc lengths, and its derivative is calculated straightforwardly:

$$E_s = \int_0^1 \sqrt{\underline{x}(\theta)^2 + \underline{y}(\theta)^2} d\theta - 1; \quad (15a)$$

$$E_s = \frac{4(1 + \frac{1}{2})}{k} E \frac{2^{p-1}}{1 + \frac{1}{2}} - 1; \quad (15b)$$

$$\frac{\partial E_s}{\partial k} = \frac{2}{k} \left[-\frac{1}{k} K \frac{2^{p-1}}{1 + \frac{1}{2}} + \frac{+1}{k} E \frac{2^{p-1}}{1 + \frac{1}{2}} \right]; \quad (16)$$

Herein, K and E are complete elliptic integrals of the first and second kind, respectively, defined by

$$K(u) = \int_0^{\frac{\pi}{2}} \frac{dx}{\sqrt{1 - u^2 \sin^2 x}}; \quad (|u| < 1); \quad (17a)$$

$$E(u) = \int_0^{\frac{\pi}{2}} \frac{dx}{\sqrt{1 - u^2 \sin^2 x}}; \quad (|u| < 1); \quad (17b)$$

The result (16) simplifies to $\frac{\partial E_s}{\partial k} = \frac{4}{k}$ in the fully cusped limit, i.e., for $p = 1$.

For later simplifications we set

$$N(\theta) := \frac{2}{k} \left[(1 - \frac{1}{2}) K \frac{2^{p-1}}{1 + \frac{1}{2}} + (+1) E \frac{2^{p-1}}{1 + \frac{1}{2}} \right];$$

leading to

$$\frac{\partial E_s}{\partial k} = \frac{N(\theta)}{k}; \quad (18)$$

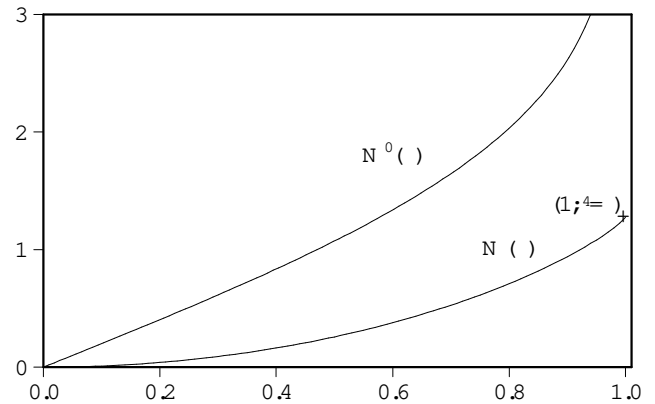


FIG. 2: The function $N(\theta)$ and its derivative.

In Fig. 2, we plot the function $N(\theta)$ and its derivative $dN(\theta)/d\theta = \frac{4}{k} K \frac{2^{p-1}}{1 + \frac{1}{2}} = \frac{4}{k} N'(\theta)$. First, we note that $N(\theta)$ is monotonously increasing from $N(0) = 0$ to $N(1) = \frac{4}{k}$. Second, the derivative diverges logarithmically near $\theta = 1$. At $\theta = 0$, $N(\theta)$ is regular, and the first few terms of its Taylor series are given by

$$N(\theta) = \frac{2}{k} \theta + \frac{1}{8} \theta^4 + \frac{3}{64} \theta^6 + \frac{25}{1024} \theta^8 + O(\theta^{10}); \quad (19)$$

This expansion will become useful later in the discussion of the type of bifurcation at the instability threshold.

To obtain the energy minimum, we simply have to solve

$$\frac{\partial E_e}{\partial k} + \frac{\partial E_s}{\partial k} = \frac{2}{k} - \frac{1}{k} + \frac{N(\theta)}{2} = 0; \quad (20)$$

The complete branch is obtained by solving Eq. (20) for k instead of θ , taking into account that θ is running from zero to one:

$$k = \frac{2}{N(\theta)}; \quad (21)$$

The solution, additionally converted to θ via equation (5) for easier comparison, is shown in figure 3. At the analytical termination point θ differs by about 11% from the numerical solution [3].

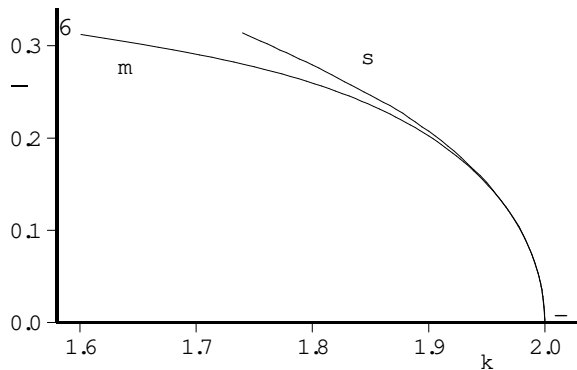


FIG. 3: The solution of the mono-cycloid model (m) in comparison with the digitized and scaled solution branch of Spencer and Meiron (s).

We immediately conclude that the termination point, given by the cusp limit $\epsilon = 1$, is located at $k = \sqrt{2}$, which is somewhat different from the termination point of Spencer and Meiron [3] at about 1.74 (their scalings imply double wave number and half amplitude with respect to ours, so they gave the termination point at $k = 3.48$).

From Eq. (5) we find using $k_{\text{term}} = \sqrt{2}$

$$\frac{\epsilon}{\text{term}} = \frac{1}{\sqrt{2}} : \quad (22)$$

An important question is the stability of our solutions. Again, only a simple calculation needs to be performed: Take k from equation (21), and plug it into the second derivative. This leads to

$$\begin{aligned} \frac{k}{2} \frac{\partial^2 E}{\partial \epsilon^2} &= \frac{1}{k} \frac{N(\epsilon)}{2^2} + \frac{N^0(\epsilon)}{2} = \frac{N(\epsilon)}{2} + \frac{N^0(\epsilon)}{2} \\ &= \frac{2}{\sqrt{2}} \frac{1+\epsilon}{2} E \frac{2^{p-1}}{1+\epsilon} + \frac{1}{(1+\epsilon)^2} K \frac{2^{p-1}}{1+\epsilon} ; \quad (23) \end{aligned}$$

which is positive for any $\epsilon \in (0;1)$. Hence the complete solution branch is stable up to the singularity, a result that agrees with that of Spencer and Meiron [3]. Of course, with our method statements about stability can be made only concerning the restricted set of functions used in the variational ansatz (which depends on just one parameter here).

Beyond $\epsilon = 1$, Eq. (20) still gives us a stationary point of the energy (even a minimum for not too far above 1), but the corresponding cycloid self-intersects, hence the solution is unphysical. Therefore, the variational ansatz provides a transparent analytic explanation of the fact that the solution branch terminates.

III. INCLUDING GRAVITY

The next natural step is the incorporation of gravity into the model. Again, the calculation of the corresponding energy contribution is fairly easy, because up to a

prefactor it is nothing but the square of the mean square amplitude.

$$E_g = \frac{l_{12}}{2} \int \underline{x}(\epsilon) \underline{y}(\epsilon) d\epsilon = \frac{l_{12}}{4} \frac{2}{k^3} \frac{2}{k^2} \quad (24)$$

Consequently, the derivative is

$$\frac{\partial E_g}{\partial \epsilon} = \frac{l_{12}}{k^3} \frac{1}{\epsilon^2} ; \quad (25)$$

and for the generalized model we replace Eq. (20) by

$$\frac{\partial}{\partial \epsilon} (E_e + E_s + E_g) = 0 : \quad (26)$$

Again it turns out that the solution can be written down exactly if we express k through ϵ . Of course, we now have two solutions which are both meaningful.

$$k = \frac{\epsilon^2}{N(\epsilon)} \frac{1}{1 + \frac{1}{N(\epsilon)} \frac{1}{2} l_{12}} \quad (27)$$

As in the no-gravity case we construct solution branches now by fixing l_{12} and then calculating $(k; \epsilon)$ pairs which may then be converted via Eq. (5) into $(k; \bar{\epsilon})$ pairs.

Hence it turns out that only the solutions for $l_{12} \in [0;1]$ cover the whole range $\epsilon = 0 :: 1$, while in the region $l_{12} > 1$, i.e., below the critical point, the system is linearly stable and hence we find no solutions close to zero. In these cases it is necessary to first calculate the minimum possible value of ϵ by demanding that the radicand in Eq. (27) shall be zero.

Clearly, the fact that finite-amplitude solutions exist at subcritical values of l_{12} is already indicative of the subcriticality of the bifurcation at the threshold, a result first obtained by Nozieres [8]. Let us discuss the vicinity of the critical point in some more detail. The neutral mode emerging at that point has of course $\epsilon = 0$. So we should expand the energy or its derivative for small ϵ to obtain the solution behavior at the bifurcation. Using Eq. (19), we find for the derivative of the total energy:

$$\begin{aligned} \frac{k}{2} \frac{\partial E}{\partial \epsilon} &= \frac{1}{k} + \frac{1}{2} + \frac{l_{12}}{2k^2} + \frac{1}{16} \frac{l_{12}}{2k^2} \epsilon^3 \\ &\quad + \frac{3}{128} \epsilon^5 + \frac{25}{2048} \epsilon^7 + \dots : \quad (28) \end{aligned}$$

At the bifurcation point, the linear term vanishes, because $k = 1$ and $l_{12} = 1$. The third-order term is negative, becoming equal to $\epsilon^3/16$, whereas higher-order terms are positive. This is to be contrasted with the Nozieres calculation and its extension by ourselves in I, showing that all the calculable coefficients of an amplitude expansion in terms of Fourier modes are negative. From this phenomenon we concluded that there is no restabilization at finite amplitude. At first sight, the situation seems to be different here, due to the positivity of

higher-order coefficients. But in fact, it is not, because the maximum meaningful amplitude is $\epsilon = 1$, and it is easy to see that for this value the third-order coefficient remains dominant. As $\epsilon \rightarrow 1$, the energy derivative tends to the negative value $4 - 2\epsilon$. In a sense, this consideration shows a little more than the calculation in terms of Fourier modes: restabilization of the structure would be possible at $\epsilon > 1$, but this is an unphysical situation.

Figure 4 shows an example for the profile of a steady state-solution taken from the critical branch ($l_2 = 1$). The solution shows the typical behavior predicted by Nozieres, i.e., at cell tips and sharp grooves. It is however unstable, as shall be seen from the discussion below.

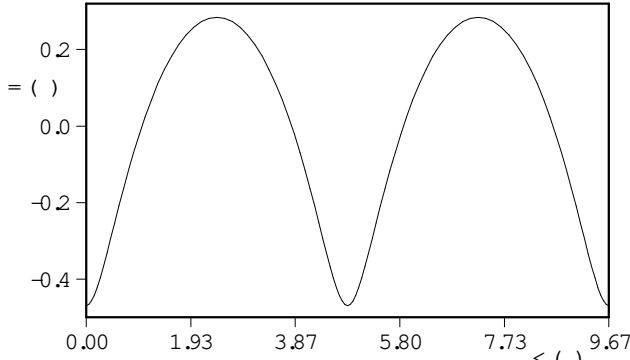


FIG. 4: Two periods of a sample solution at $k = 1.3, \epsilon = 0.25$ (which corresponds to $\epsilon = 0.49$).

A number of solution branches for different values of l_2 is shown in Fig. 5. In this plot, we first of all see how the range of unstable wave numbers, starting with the interval $(0; 2)$ becomes narrower with increasing l_2 , i.e., higher gravity or lower prestress. At $l_2 = 1$ only a single k value remains unstable; this is the critical case in the model with gravity.

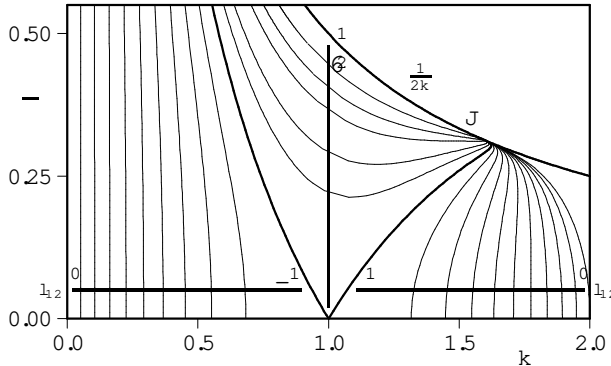


FIG. 5: Solution branches of equation (26) for different values of l_2 . The rightmost curve, beginning at $(k; l_2) = (2.0; 0.0)$, is the no-gravity solution shown in Fig. 3. A row of small numbers denote l_2 values corresponding to the curves. The upper bold line is the limiting curve for large l_2 . The common termination point of all branches is marked by a circle. For more details of this region see Fig. 6.

At even higher values of l_2 we are in the subcritical range where it takes some energy to modulate the sur-

face in order to overcome the energy barrier to let the instability emerge. In Fig. 5 we have shown solutions up to $l_2 = 2$. The solution branches converge towards $\epsilon = 1 = 2k$ as l_2 is increased, which is the transformation of the cusp limit $\epsilon = 1$ (see equation 5). The common endpoint of all curves ($\epsilon = 1$) is marked with a circle.

Again, as in the no-gravity case we have to check the stability of the solutions by putting the corresponding solution (27) into the second derivative of the energy. First we note that all branches left of $k = \epsilon/2$ in Fig. 5 start off unstably. But there is a range of stability which we discuss with the help of Fig. 6 rather than 5.

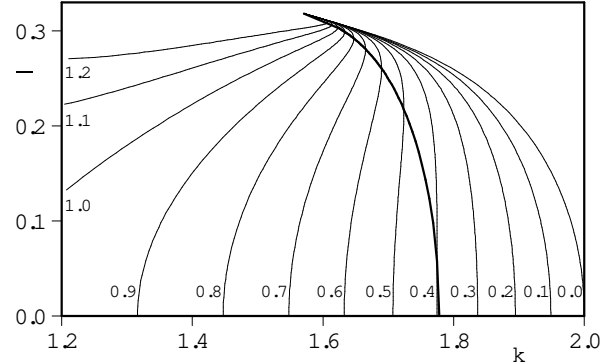


FIG. 6: Solution branches of equation (26) in a certain k -range. The region bounded by the no-gravity solution and the curve (thick line) from the bullet symbol up to the cusp point contains the stable solutions.

In this figure, we have included the range of stable solutions. The largest l_2 value where all solutions still emerge stably ($\epsilon = 1$) is $l_2 = 32/81$, corresponding to $k = 16/9$. This is to be contrasted with the result of I, where the tricritical point is shown to be located at $k = 13/57 = 0.228$, corresponding to $l_2 = 20/57 = 0.351$. Because the result from the amplitude equations is exact at infinitesimal amplitudes, the variational ansatz overestimates the range of supercritical bifurcation at lowest order. Of course, such a comparison is a bit unfair towards the variational approach, as we have only a single parameter available there, whereas the lowest-order nonlinear mode expansion contains already two amplitudes. As soon as we take the multi-cycloid ansatz, discussed below, to second order, we obtain the exact position of the tricritical point within this ansatz as well. This is simply due to the fact that the multi-cycloid contribution of order n does not contain Fourier modes lower than n (see Eq. 29).

An interesting fact is the bending of all solution branches into a stable region before running into the cusp, a feature not obtained within the amplitude equation approach (compare Fig. 7 of I with Fig. 6). Actually, the stability changes right where the slope turns negative (passing from $+1$ to -1). This can be interpreted as a hint for the existence of stable solution branches at high gravity. These stable solutions do not, at least in the mono-cycloid approximation, emerge at the upper marginal wave number $1 + \sqrt{1 - l_2}$ predicted by linear

theory but instead in the (upper) vicinity of $k = \pi$ at nonzero amplitude. Whether this is really true will be checked in the following chapters by the implementation of the multi-cycloid ansatz.

IV. THE MULTI-CYCLOID APPROXIMATION

The multi-cycloid model is a natural generalization of the cycloid from ansatz (1):

$$\underline{x}(z) = \sum_{n=1}^N \frac{X_n}{nk} e^{ink} z; \quad (29)$$

Herein, N is the maximum number of "cycloid modes" taken into account. The denominator n in this equation which could also have been integrated into the definition of the X_n has been explicitly written in order to be able to express the generalized cusp condition in a compact way. Real and imaginary parts read:

$$x(z) = \sum_{n=1}^N \frac{X_n}{nk} \sin(nkz); \quad (30a)$$

$$y(z) = \sum_{n=1}^N \frac{X_n}{nk} \cos(nkz); \quad (30b)$$

Again we shift the interface by its mean value to set the average interface position equal to zero:

$$m = \frac{k}{2} \int_0^Z \underline{x}(z) y(z) dz = \frac{1}{2k} \sum_{n=1}^N \frac{X_n^2}{n}; \quad (31)$$

and we have to correct Eq. (30b) as follows:

$$y(z) = \sum_{n=1}^N \frac{X_n}{nk} \cos(nkz) + \frac{n}{2}; \quad (32)$$

Moreover, we will need the mean square amplitude again. The result is

$$\overline{u^2} = \frac{1}{k} \sum_{n=1}^N \frac{X_n^2}{2n^2} + \frac{1}{2} \sum_{j=1}^N \frac{X_j^2}{j} + \frac{1}{2} \sum_{j=1}^N \frac{X_j^2}{j(j+n+j)}; \quad (33)$$

We assume the sequence of the X_n to decrease sufficiently fast so the sum of the absolute values of the X_n does not exceed one, a condition that is sufficient to avoid self-crossings of the curve given by (29). Then cusps, if they exist, can appear only at

$$z_{\text{cusp}} = k = 2\pi n; \quad n \in \mathbb{N}; \quad (34)$$

(They are characterized by $\dot{y}(z) = 0$.) The curvature radius is given as [9]

$$r = \frac{\sqrt{\dot{x}^2 + \dot{y}^2}^{\frac{3}{2}}}{\dot{x}(z)\dot{y}(z)}; \quad (35)$$

and it takes its minimum value at $z = z_{\text{cusp}}$. So,

$$r_{z=0} = \frac{1 + \sum_{n=1}^N \frac{X_n^2}{k^2 n^2}}{k \sum_{n=1}^N \frac{X_n}{n}}; \quad (36)$$

and the cusp condition reads

$$\sum_{n=1}^N \frac{X_n}{n} = 1; \quad (37)$$

Now the derivatives of the relevant energies have to be calculated. Note that the integration for the energies themselves may not be carried out analytically for general multi-cycloids. But the question of stability of the solution can be answered because first and second derivative can be given explicitly.

The crucial point is the calculation of the elastic energy density $w(s)$ at the surface, which is done in appendix A. Supposing $w(s)$ is given (see Eq. (A15)), we have to modify Eqs. (10) and (11) as follows (we write C_n and S_n instead of $\cos(nkz)$ and $\sin(nkz)$):

$$\begin{aligned} \underline{x} &= \sum_{n=1}^N \left[\frac{\partial x(z)}{\partial z} e_x + \frac{\partial y(z)}{\partial z} e_y \right] z \\ &= \frac{1}{nk} \sum_{n=1}^N [S_n e_x + (C_n + n) e_y] z; \end{aligned} \quad (38)$$

$$nds = (y(z) e_x + x(z) e_y) dz \quad (39)$$

Consequently, we get according to Eq. (9)

$$\frac{\partial E_e}{\partial n} = \frac{1}{nk} \int_0^Z w(s) [S_n y(z) - (C_n + n) x(z)] dz; \quad (40)$$

The other terms are simpler again. Gravitational energy is $\frac{1}{2} \int_0^Z u^2 dz$ times the square of the mean square amplitude (33):

$$E_g = \frac{1}{2} \int_0^Z u^2 dz; \quad (41)$$

and hence

$$\begin{aligned} \frac{\partial E_g}{\partial n} &= \frac{1}{2k^2} \int_0^Z u^2 dz \\ &= \frac{1}{2k^2} \sum_{j=1}^N \frac{X_j^2}{j} + \frac{1}{2} \sum_{j=1}^N \frac{X_j^2}{j(j+n+j)}; \end{aligned} \quad (42)$$

and the surface tension is again represented by the difference of the arc lengths (compare Eq. (15a)), hence its derivative reads after some simplification

$$\frac{\partial E_s}{\partial \tau} = \frac{\partial}{\partial n} \left[\sum_{l=1}^N \left(1 + \frac{X^N}{1 + 2C_1} \right) + 2 \sum_{l=1}^N \sum_{j=1}^N C_{1j} \right]; \quad (43)$$

This integral can only be solved analytically for the case $N = 1$, as has been shown in the mono-cycloid model.

Equipped with the terms (40), (42) and (43) we can now numerically solve the system

$$\frac{\partial}{\partial n} (E_e + E_s + E_g) = 0; \quad n = 1 :: N; \quad (44)$$

for the set $f_1 :: N g$, given a certain prescribed k value. Some technical details of the solution method are given in appendix B.

We have carried out the calculations for $N = 1$ (mono-cycloids) as well as $N = 2$ and $N = 3$. Figure 7 shows how fast the solution branches converge to the numerical result from [3].

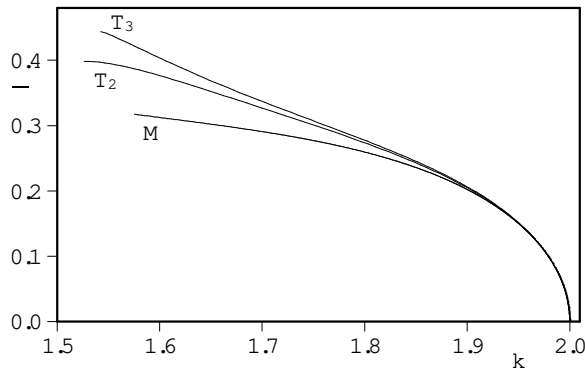


FIG. 7: Comparison of the $N = 1; 2$ and 3 multi-cycloid models in the no-gravity case. The termination points $T_{n,m}$ marked with an open circle, are not the cusp points. T_2 is the point of minimal curvature radius, as at least in the double cycloid model the cusp is actually not reached. The solutions turn into bag-like morphologies left of T_2 instead (i.e., they develop overhangs). T_3 is the point where our numerics stops. At this point we have $\tau_1 = 0.9989$, i.e. we are slightly before the cusp. For the mono-cycloid an analytically exact solution (M) is known. The stars represent the numerical solution from [3], terminating at the point denoted by $*$.

Another means for the determination of the quality of the solution is the curvature radius in the minimum of the grooves which has to approach zero. Here we note a remarkable behavior (Fig. 8). Although we find an increasing quality of the mean square amplitude branch with higher N , it takes $N = 3$ to improve the solution for the curvature radius over that for $N = 1$.

This improvement of the third order with respect to the first one happens only for $k \gtrsim 1.75$; for smaller k

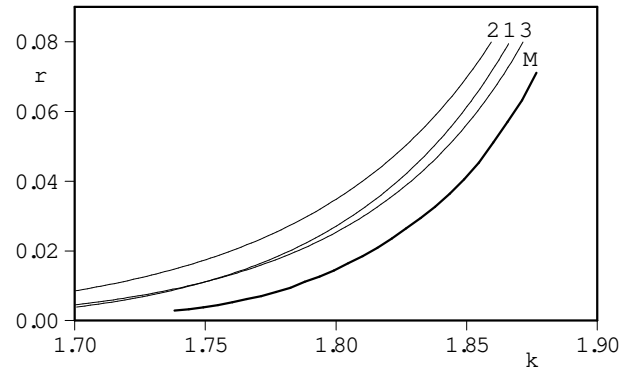


FIG. 8: Curvature radii for $N = 1, 2$ and 3 . explanations see text. The bold line shows the digitized and scaled curvature radii of the Spencer solution.

the mono-cycloid model gives the smallest radius. This result can be interpreted as follows: either, third order multi-cycloid approximation is insufficient for a correct description of the groove shape or the solution of Spencer and Meiron, which yields the same mean square amplitude like ours, underestimates the length of the solution branch because of the restricted number of modes they used. Since they are resolving a much smaller curvature radius than the one obtained with our approximation at $k \approx 1.75$, the first interpretation seems more likely.

The incorporation of gravity has been carried out up to $l_{12} = 1$. Figure 9 gives the solution branches, unstable curves left of $k = 1$ are not shown. We note that the common cusp point, an important feature of Fig. 6, disappears. As in Fig. 7, the curves terminate before the cusp is actually reached.

Stability of the solutions is checked via computation of the determinant of the matrix $\partial^2 E = \partial_n \partial_m$ and its principal minors. If all of these are positive, the matrix is positive definite, the energy has a minimum and the solution is stable. As it turns out, the determinant itself gets positive only after its minors, so it would in our case be sufficient to check the sign of the determinant alone. The onset of stability is shown in Fig. 9 by means of circles. We conclude that the stability behavior is qualitatively correctly described by the mono-cycloid model already. However, stability sets in at smaller amplitudes for k values below 1.7. Hence, the multi-cycloid modes act stabilizing at larger amplitudes and destabilizing near the tricritical point, which is shifted to larger k by inclusion of modes beyond the mono-cycloid.

Finally, in Fig. 10, we present a stable and an unstable pattern on the same solution branch ($l_{12} = 0.6$) and at the same k -value (1.69, see the diamond symbols in Fig. 9).

The figure shows that up to the different distances to the cusp, which make the curves more or less "sharp", there is no indication from the shape itself whether it is stable or not. Small-amplitude stable solutions at larger k just look like the unstable solution B from Fig. 10.

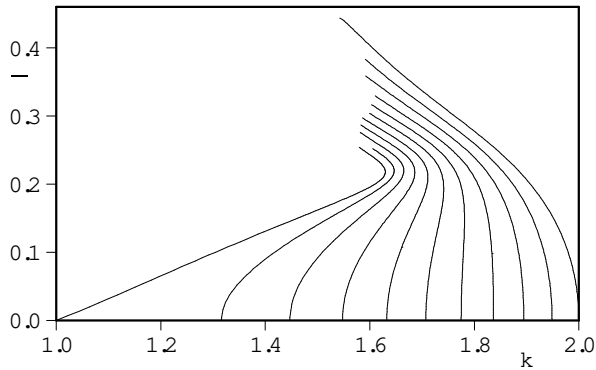


FIG. 9: Solution branches based on the $N = 3$ multi-cycloid model from $l_2 = 0$ (rightmost) to 1 (left). Circles mark the beginning of the region of stability, reaching up to the termination points. The diamonds refer to the curves in g. 10.

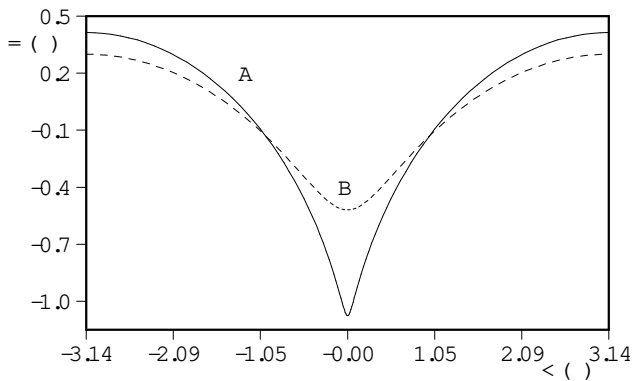


FIG. 10: A stable (A, straight) and an unstable pattern (B, dashed), at $k = 1.69$ and $l_2 = 0.6$.

V. SUMMARY

To conclude, we have presented a variational approach to the calculation of steady states for the Grinfeld instability. Taking into account a single mode we already obtain a very nice qualitative description of the system behavior including the approach to a cusped state. The wavenumber for the cusp appearance is not accurate with a single mode. Nevertheless, this single mode approximation has the virtue of great transparency. That a cusp singularity appears is rendered understandable: the system simply draws near a state where further minimization of the elastic energy would require the interface to self-intersect.

Even the one-mode approximation suggests the existence of stable large-amplitude steady states in the presence of gravity, as is demonstrated by Fig. 6. Taking into account three modes, we obtain a quantitatively satisfactory description of the numerical Spencer-Meiron branch, conveying some confidence that the new branches with gravity are equally well described by the three-mode approximation. The stability domain suggested by the one-mode picture is roughly confirmed in the three-mode representation (see Fig. 9). As gravity is increased, there are no small-amplitude stable solutions anymore. At

first sight, this might seem counterintuitive: why should gravity, a stabilizing effect, destroy the stability of small-amplitude solutions? The answer is that gravity renders the zero-amplitude, i.e. planar, solution more stable and hence larger amplitudes are needed for true structures to become stable.

Hence, we conclude that in confined systems under gravity or a similar body force (it has been shown that in directional solidification a temperature gradient acts just as a strong effective gravity field [10, 11]) stable steady states may exist at large amplitude and be absent at small ones.

Below the instability threshold, i.e., for parameters where the planar interface is stable, the system may be forced into a large amplitude state. This clearly calls for numerical simulations and experimental attempts at creating these states.

Acknowledgments

This work was supported by the Deutsche Forschungsgemeinschaft under Grant No. Ka 672/4-2 and FOR 301/2-1, which is gratefully acknowledged. In addition, we acknowledge travel grants by PROCOPE, Grant No. 9619897 (DAAD, Germany) and 97176 (APAPE, France), enabling a closer collaboration between the two groups involved in this work.

APPENDIX A: CALCULATION OF THE STRAIN ENERGY DENSITY ALONG A MULTI-CYCLOID SURFACE

Instead of calculating the strain energy density inside the bulk as we did in I, we will only describe here how to calculate this energy density $w(s)$ at the surface. We carry out the calculation for general N -cycloids.

In general, the elastic energy density of a solid submitted to plane strain can be written in terms of the two-dimensional stress tensor as

$$w = \frac{1}{2E} \sum_{ij} \sum_{kk} \sigma_{ij} \sigma_{kk}; \quad (\text{A1})$$

where summation over repeated subscripts is implied. At the interface, σ_{ij} is diagonal with elements σ_{tt} and σ_{nn} . Since $\sigma_{tt} = \text{Tr} \sigma_{nn}$ and because in our normalization $\sigma_{nn} = 0$, the elastic energy density can be expressed by the trace of the stress tensor alone, which allows us to deal with a single scalar. Thus the strain energy density takes the form

$$w(x;y) = \frac{1}{2} (\text{Tr} \sigma)^2; \quad (\text{A2})$$

where $\text{Tr} \sigma$ is in our non-dimensional scalings equal to $1 + \sigma_{xx} + \sigma_{yy}$.

The idea is to employ a mapping of the half-plane bounded from above by our multi-cycloid onto the area

below the real axis using the analytic function

$$z = !(\xi) = \xi - i \sum_{n=1}^{\infty} \frac{X^n}{nk} e^{ink\xi} \quad (A 3)$$

where $\xi = x + iy$. This defines a mapping of the domain $z = (x, y)$ to the lower ξ half plane, as can be seen easily by restricting to $y = 0$ which shows that the interface is mapped to the real axis. In order to solve the elastic problem we have to satisfy [7]

$$\phi_0(\xi) + [\psi(\xi) - \overline{\psi(\xi)}] \frac{\overline{\phi_0(\xi)}}{\overline{\psi(\xi)}} + \frac{\overline{\phi_0(\xi)}}{\overline{\psi(\xi)}} = \frac{\overline{\psi(\xi)} - \psi(\xi)}{2}; \quad (A 4)$$

where ϕ_0 and ψ_0 are modified Goursat functions. These functions must be analytic for $|\xi| > 1$, so it has to be established that $\frac{\overline{\phi_0(\xi)}}{\overline{\psi(\xi)}}$ contains no exponentials increasing for $|\xi| > 1$ when ξ is replaced by $x + iy$. Since $\frac{\overline{\phi_0(\xi)}}{\overline{\psi(\xi)}}$ is the complex conjugate of a function that is analytic in the lower half plane, it must be analytic in the upper half plane, which means that terms of the form $\exp(in\xi)$ are allowed whereas $\exp(-in\xi)$ are not (for details see [7]). For brevity, we will designate the forbidden terms as "negative exponentials". Technically, we make an ansatz for $\phi_0(\xi)$:

$$\phi_0(\xi) = \sum_{n=1}^{\infty} \frac{i X^n}{k} c_n e^{ink\xi}; \quad (A 5)$$

where we may assume c_n to be real (which will be justified later). Now let us simplify Eq. (A 4). We have

$$[\psi(\xi) - \overline{\psi(\xi)}] = 2i\psi(\xi) = \frac{2i X^n}{k} \sum_{n=1}^{\infty} \frac{c_n}{n}; \quad (A 6)$$

and hence

$$\frac{\overline{\phi_0(\xi)}}{\overline{\psi(\xi)}} = \sum_{n=1}^{\infty} \frac{X^n}{k} \frac{c_n}{n} + \frac{\overline{\phi_0(\xi)}}{\overline{\psi(\xi)}} \phi_0(\xi); \quad (A 7)$$

Via the choice of c_n we have to establish that the right hand side of Eq. (A 7) contains no negative exponentials. Let us further simplify the representation. We have

$$\frac{\overline{\phi_0(\xi)}}{\overline{\psi(\xi)}} = \sum_{n=1}^{\infty} c_n e^{ink\xi}; \quad (A 8a)$$

$$\overline{\psi(\xi)} = \sum_{n=1}^{\infty} e^{ink\xi}; \quad (A 8b)$$

For the division, we use the common expression for the quotient of two series ([12], p.28): Let

$$\begin{aligned} s_1 &= 1 + a_1 x + a_2 x^2 + a_3 x^3 + \dots; \\ s_2 &= 1 + b_1 x + b_2 x^2 + b_3 x^3 + \dots; \\ s_3 &= 1 + c_1 x + c_2 x^2 + c_3 x^3 + \dots; \\ s_4 &= 1 + d_1 x + d_2 x^2 + d_3 x^3 + \dots; \\ s_5 &= 1 + e_1 x + e_2 x^2 + e_3 x^3 + \dots; \end{aligned}$$

with

$$s_1 = 1 + \frac{X^0}{0}(\xi); \quad s_2 = \overline{\psi(\xi)};$$

that is

$$a_n = n c_n; \quad b_n = c_n; \quad x = e^{ik\xi};$$

We then need to calculate

$$\begin{aligned} s_3 &= \frac{s_1}{s_2}; \\ s_4 &= s_2^{-1}; \\ s_5 &= s_3 s_4 = \frac{\overline{\phi_0(\xi)}}{\overline{\psi(\xi)}}; \end{aligned}$$

The coefficients c_n and d_n are given by the recursion

$$\begin{aligned} c_1 &= a_1 - b_1; \\ c_n &= a_n - 4b_n + \sum_{j=1}^{n-1} b_j c_{n-j}; \\ d_1 &= b_1; \\ d_n &= 4b_n + \sum_{j=1}^{n-1} b_j d_{n-j}; \end{aligned}$$

This leads to

$$\begin{aligned} c_1 &= a_1; \\ c_n &= a_n - \sum_{j=1}^{n-1} b_j c_{n-j}; \end{aligned} \quad (A 9)$$

We then have, after introducing $\phi_0 = \psi_0$,

$$1 + 2 \frac{\overline{\phi_0(\xi)}}{\overline{\psi(\xi)}} = 1 + 2s_5 = 2 \sum_{n=0}^{\infty} c_n x^n; \quad (A 10)$$

Therefore,

$$\begin{aligned} c_0 &= \frac{1}{2}; \quad c_1 = 0; \\ c_n &= n c_{n-1} + \sum_{j=1}^{n-1} c_j c_{n-j}; \quad n = 2 :: N; \end{aligned} \quad (A 11)$$

Negative exponentials on the right-hand side of (A 7) can only result from the negative exponentials in

$$c_n = \frac{1}{2} e^{ink\xi} + e^{-ink\xi};$$

We cut out the relevant parts from Eq. (A 7), consisting of negative exponentials and require them to become zero, to compute the coefficients determining ϕ_0 in terms of the c_n

$$\sum_{m=1}^{\infty} \frac{X^m}{m} e^{imk\xi} \otimes \sum_{j=0}^{\infty} c_j e^{ijk\xi} A = \sum_{n=1}^{\infty} c_n e^{ink\xi}; \quad (A 12)$$

with $\phi_0 = 1/2$ and the prefactor ik^{-1} dropped. Now we sort the terms in this equation by exponentials which naturally gives us the system

$$X_n = \sum_{j=0}^{N-n} \frac{j^{n+j}}{n+j}; \quad n = 1:::N : \quad (A13)$$

Note that the X_j contain the X_i as well, so the equations are not a simple recursive scheme but a linear system of equations for the X_n . Now we get back to Tr , which

can be written as

$$Tr = 1 + 4 \frac{x(\phi) \langle \phi \rangle + y(\phi) = \langle \phi \rangle}{x(\phi)^2 + y(\phi)^2} : \quad (A14)$$

The denominator has already been written down during the calculation of the arc length. The numerator can be simplified in a similar manner. After all simplifications have been performed, we finally get

$$w(s) = \frac{1}{2} \frac{6}{4} 1 + 4 \frac{\sum_{n=1}^N C_n \sum_{j=1}^{N-n} (j^{j+n} (j+n) + j^{j+n} j)}{1 + \sum_{n=1}^N C_n (2C_n) + 2 \sum_{n=1}^N C_n \sum_{j=1}^{N-n} j^{j+n}} : \quad (A15)$$

APPENDIX B: DETAILS OF THE NUMERICAL SOLUTION OF EQ. (44)

Let us first repeat the system of partial differential equations (44).

$$\frac{\partial}{\partial x_j} [E_e + E_s + E_g] = 0; \quad j = 1:::N : \quad (B1)$$

Herein, the energy changes entering the equation are integrals over certain rational terms containing trigonometrical functions and the vector of amplitudes $\underline{a} = (a_1;:::a_N)$ as well as the wave number k . The generic method of solution would be to fix the wave number and then to solve the coupled algebraic equations numerically (B1) for \underline{a} . Using the following method we can considerably reduce the numerical effort in the solution.

We reformulate the problem (B1) by considering the fact that k is contained in the energy terms as a prefactor only (compare Eqs. (40), (42) and (43)) [4]. Then we get a simplified problem with modified E terms:

$$\frac{\partial}{\partial x_j} \left[\frac{1}{k} E_e(\underline{a}) + E_s(\underline{a}) + \frac{1}{k^2} E_g(\underline{a}) \right] = 0 : \quad (B2)$$

We define the abbreviations

$$1;j = \frac{\partial E_e(\underline{a})}{\partial x_j}; \quad 2;j = \frac{\partial E_s(\underline{a})}{\partial x_j}; \quad 3;j = \frac{\partial E_g(\underline{a})}{\partial x_j}$$

If we now fix k , then for any equation of the system (B2) the equation

$$k = \frac{1}{2} \frac{1;j \sum_{i=1}^N (1;j)^2 + 4 \sum_{i=1}^N 2;j 3;j}{2;j} = : \quad j \quad (B3)$$

holds. That's why we can fix one amplitude (a_1 without restriction of generality) and calculate the others by the reduced system

$$a_j = 0; \quad j = 2:::N : \quad (B4)$$

The value of k is determined by the choice of a_1 . It can be calculated from (B3) after solution of (B4). This is done numerically by minimisation of a term

$$f(\underline{a}) = \sum_{j=2}^N (a_j - 1)^2; \quad (B5)$$

which becomes zero at the exact solution and is numerically calculated to a limit of typically 10^{-10} . It is necessary to choose a good starting approximation which can be derived by polynomial interpolation from close-by data points. After that, one seeks in the space spanned by $a_2:::a_N$ for the direction where $f(\underline{a})$ takes its steepest descent.

For a wide range of parameters this calculation scheme is numerically more efficient than the implemented Maple solver. But in the vicinity of the cusps it crashes. Instead, it is useful there to switch to the direct solution of the system

$$a_j = 0; \quad j = 2:::N ; \quad (B6)$$

at fixed a_1 using `fsolve`.

There is also a disadvantage. As we go into a direction of the solution branch estimated from the points before, this method will in general not find bifurcations.

-
- [1] W. Yang and D. Srolovitz, *Phys. Rev. Lett.* 71, 1593 (1993).
- [2] K. Kassner and C. Misbah, *Europhys. Lett.* 28, 245 (1994).
- [3] B. Spencer and D. Meiron, *Acta Metall. Mater.* 42, 3629 (1994).
- [4] C.-H. Chiu and H. Gao, *International Journal of Solids and Structures* 30, 2983 (1993).
- [5] N. I. Muskhelishvili, *Einige Grundaufgaben zur mathematischen Elastizitätstheorie* (Fachbuchverlag, Leipzig, 1971).
- [6] P. Kohlert, K. Kassner, and C. Misbah, *Phys. Rev. E* (2002), to be published.
- [7] K. Kassner, C. Misbah, J. Müller, J. Kappey, and P. Kohlert, *Phys. Rev. E* 63, 036117 (2001).
- [8] P. Nozières, *J. Phys. I France* 3, 681 (1993).
- [9] H.-J. Bartsch, *Mathematische Formeln* (Buch- und Zeitungsverlagsgesellschaft mbH, Köln, 1988), 15th ed.
- [10] I. Durand, K. Kassner, C. Misbah, and H. Müller-Krumhaar, *Phys. Rev. Lett.* 76, 3013 (1996).
- [11] I. Cantat, K. Kassner, C. Misbah, and H. Müller-Krumhaar, *Phys. Rev. E* 58, 6027 (1998).
- [12] M. Abramowitz and I. A. Stegun, eds., *Pocketbook of Mathematical Functions* (Harri Deutsch, Thun, Frankfurt/Main, 1984), abridged Edition of "Handbook of Mathematical Functions".
- [13] This is not a superposition in the standard sense. We add up (partial) parametric representations of the x and y coordinates, so the whole curve is not a simple sum, see Eq. (29).
- [14] De facto we have also transformed the integration variable $X = k$, changing the integration interval to $[0; \dots]$.